Asteroseismology of the ZZ Ceti star HS 0507+0434B[⋆⋆]

J.-N. Fu[1]†; N. Dolez[2,3]; G. Vauclair[2,3]; L. Fox Machado[4]; S.-L. Kim[5]; C. Li[1];
L. Chen[1]; M. Alvarez[4]; J. Su[6]; S. Charpinet[2,3]; M. Chevreton[7]; R. Michel[4];
X.H. Yang[1]; Y. Li[6]; Y.P. Zhang[1]; L. Molnar[8,9] and E. Plachy[8,9]

[1]*Department of Astronomy, Beijing Normal University, Beijing, China*

[2]*Université de Toulouse,UPS-OMP, IRAP, Toulouse, France*

[3]*CNRS, IRAP, 14 avenue E. Belin, 31400, Toulouse, France*

[4]*Observatorio Astronómico Nacional, Instituto de Astronomía, Universidad Nacional Autónoma de México, Ensenada, B.C., México*

[5] *Korea Astronomy and Space Science Institute, Daejon, Korea*

[6]*Yunnan Astronomical Observatory, Chinese Academy of Sciences, Kunming, China*

[7]*LESIA, Observatoire de Paris-Meudon, Meudon, France*

[8]*Konkoly Observatory, MTA CSFK, H-1121, Konkoly-Thege u 15-17, Budapest, Hungary*

[9]*Eötvös University, H-1117 Budapest, Pázmány Péter sétány 1/a, Hungary*

ABSTRACT

The pulsating DA white dwarfs (ZZ Ceti stars) are *g*-mode non-radial pulsators. Asteroseismology provides strong constraints on their global parameters and internal structure. Since all the DA white dwarfs falling in the ZZ Ceti instability strip do pulsate, the internal structure derived from asteroseismology brings knowledge for the DA white dwarfs as a whole group. HS 0507+0434B is one of the ZZ Ceti stars which lies approximately in the middle of the instability strip for which we have undertaken a detailed asteroseismological study. We carried out multisite observation campaigns in 2007 and from December 2009 to January 2010. In total, 206 hours of photometric time-series have been collected. They have been analysed by means of Fourier analysis and simultaneous multi-frequency sine-wave fitting. In total, 39 frequency values are resolved including 6 triplets and a number of linear combinations. We identify the triplets as ℓ=1 *g*-modes split by rotation. We derived the period spacing, the rotational splitting and the rotation rate. From the comparison of the observed periods with the theoretical periods of a series of models we estimate the fundamental parameters of the star: its total mass $M_*/M_\odot$ = 0.675, its luminosity $L/L_\odot$=3.5×10^{-3}, and its hydrogen mass fraction M_H/M_* = $10^{-8.5}$.

Key words: stars:white dwarfs – stars:oscillations – stars:individual:HS 0507+0434B.

1 INTRODUCTION

As the end products of about 97% of the stars of the Galaxy, white dwarf stars offer important clues about their prior evolutionary history. They also provide potentially the age of the galactic disk and of the globular clusters they belong to (Winget et al. 1987; Harris et al. 2006) through the age that can be estimated from cooling sequences (Ruiz & Bergeron 2001).

However, determining the age of a white dwarf on its cooling sequence requires knowing its fundamental parameters: the total

mass, the effective temperature, the luminosity, the fractional mass of the hydrogen and/or the helium outer layers, the core composition,etc. Asteroseismology of white dwarfs provides a unique tool to explore their internal structure and determine those fundamental parameters. The method has been successfully applied to the pulsating pre-white dwarf stars of PG 1159 type, the GW Vir stars, e.g. the prototype of the group PG 1159-035 (Winget et al. 1991), the hottest one RXJ 2117+3412 (Vauclair et al. 2002) and the coolest one PG 0122+200 (Fu et al. 2007, Córsico et al. 2007), to the DB pulsators, e.g. GD 358 (Winget et al. 1994, Provencal et al. 2009), PG 1351+489 (Redaelli et al. 2011), and to the DAV stars, either for individual pulsator, e.g. HL Tau 76 (Dolez et al. 2006) or for global study of the group properties (Castanheira & Kepler 2009; Romero et al. 2012).

Since ≈ 80% of the white dwarf stars are of DA type, the uncertainties on their fundamental parameters have a strong impact on the derived age estimates. This justifies the effort in determining

precise fundamental parameters of DA white dwarfs using astero-seimology of the DA pulsators, the DAV or ZZ Ceti stars. There are presently 148 pulsating DA white dwarfs known (Castanheira et al. 2010a, 2010b). These stars define a narrow instability strip in the H-R diagram (or in the $\log g$-T$_{eff}$ diagram). This instability strip is a "pure" instability strip, which means that all the DA white dwarfs falling in this domain of the $\log g$-T$_{eff}$ diagram do pulsate (Gianninas et al. 2011). This is an indication that the internal structure of the ZZ Ceti white dwarfs as derived from asteroseismology is representative of the DA white dwarfs as a whole group.

White dwarf stars being the oldest stars in a given stellar population, they can be used to estimate the age of the population they belong to. However, to achieve such a goal one must rely on realistic models of white dwarf stars. The major uncertainties in building such realistic models come from the uncertainty on their total mass and on their hydrogen mass fraction as well as from the approximate treatment of the convection by the mixing length theory parameterized by a mixing length α. The asteroseismology is the only method able to determine the value of the hydrogen mass fraction and to give accurate total mass estimates of the ZZ Ceti white dwarfs. In addition, new theoretical developments on the interaction of the pulsations with convection have opened a way to constrain the efficiency of the convection in white dwarf stars (Wu 2001, Montgomery 2005, Montgomery et al. 2010).

The difficulty in determining the fundamental parameters of the ZZ Ceti stars from asteroseismology comes from two main sources: 1) the ZZ Ceti stars show generally few modes simultaneously, in contrast with the theoretical calculations which predict much more unstable modes than observed, and 2) the pulsation amplitudes become increasingly variable as the ZZ Cetis evolve towards the red edge of the instability strip. Both effects make difficult to find enough appropriate modes to use the method based on the period spacing which needs a large enough number of pulsation modes to be observed and identified. Only ZZ Ceti stars close to the blue edge of the instability strip show constant pulsation amplitude. But in this case, very few modes are unstable since the stars are just entering the instability strip. In those stars, the κ-mechanism due to hydrogen partial ionization is responsible for the instability since the fraction of the flux conveyed by convection is negligible (Dolez & Vauclair 1981, Winget et al. 1982). As the white dwarfs evolve along their cooling sequence, the fraction of the flux conveyed by convection increases. The light curves become more complex as a result of the interaction of the convection with the pulsations. They show signatures of nonlinear effects like non sinusoidal pulse shapes which reflect into linear combinations of "real" frequencies in the Fourier spectrum. Modeling precisely the light curve resulting from these inteactions can be used to constrain the efficiency of convection (Montgomery 2005, Montgomery et al. 2010). The asteroseismological analysis of various ZZ Ceti stars through the instability strip allows to map the convection efficiency.

The DA white dwarf HS 0507+0434B is one of those ZZ Ceti star of particular interest which we intend to study in more details. Its parameters as derived from earlier spectroscopy give an effective temperature of 11630±200 K and $\log g$= 8.17±0.05 (Fontaine et al. 2003; Bergeron et al. 2004) which placed HS 0507+0434B approximately in the middle of the instability strip of the ZZ Ceti pulsators. Fontaine et al. (2003) provide a mass value of 0.71 $M_\odot$ derived from the models of Wood (1995) for carbon core compositions, helium layers of $M_{He} = 10^{-2}M_\star$, and hydrogen layers of $M_H = 10^{-4}M_\star$, and absolute magnitude in V of $M_V = 11^m99$. More recent high signal/noise ratio spectroscopy and atmospheric analysis by Gianninas et al. (2011) have shifted the ZZ Ceti instabil-

ity strip to higher effective temperature. With an effective temperature and a surface gravity of 12290 ±186 K and $\log g$= 8.24±0.05 respectively, HS 0507+0434B still lies close to the middle of the new ZZ Ceti instability strip. It is of particular interest because it forms a common proper motion pair with HS 0507+0434A, which is a 20000 K DA white dwarf (Jordan et al. 1998). Gianninas et al. (2011) give also a higher effective temperature of 21550 ±318 K for the A component. Since both members of the pair must have been formed at the same time, this provides one additional constraint on the modeling of their evolution.

HS 0507+0434B was discovered to be a ZZ Ceti variable by Jordan et al. (1998). It has been observed subsequently from single sites only (Kotak et al. 2002; Handler et al. 2002). Those observations allowed the detection of 10 independent frequencies identified as l=1 gravity modes and of 38 linear combinations of these frequencies (Handler et al. 2002). The linear combinations of frequencies were interpreted as resulting from the nonlinear interaction of the pulsations with convection. The 10 independent frequencies are formed of three triplets (i.e. l=1 modes split by rotation) plus one single mode. This was clearly insufficient to constrain the star internal structure. To improve this situation, we carried out multisite observation campaigns in 2007, December 2009 and January 2010 to study HS 0507+0434B.

The goal of this paper is to improve the determination of the fundamental parameters of HS 0507+0434B using the new data collected during the campaigns of 2007, 2009 and 2010. It is organized as follows: the observations are described in §2. §3 analyses the derived amplitude spectrum. A preliminary asteroseismology of HS 0507+0434B is presented in §4 where are discussed successively the frequency identification and their linear combinations, in 4.1, the period distribution and the period spacing, in 4.2, the rotational splitting and the rate of rotation, in 4.3, the inclination of the rotation axis, in 4.4, and the mode trapping in 4.5. §5 discusses the amplitude variations. From the improved list of pulsation modes resulting from this work, we attempt to constrain the fundamental parameters of HS 0507+0434B by building a set of models which are described in §6, from which we derived one "best fit" model. We summarize our results in the conclusions §7.

2   OBSERVATIONS AND DATA REDUCTION

HS 0507+0434B was observed during a one week multisite campaign in December 2007, involving the 2.16-m telescope of the National Astronomical Observatories of China (NAOC) in Xinglong (XL), the 1.8-m telescope of Bohyunsan Optical Astronomy Observatory (BOAO) of Korea and the 1-m telescope of Piszkéstető Observatory (PO) of Hungary. Later on, a four-week multisite run was carried out from December 2009 to January 2010 with the 2.16-m telescope in XL, the 2.4-m telescope of Yunnan Astronomical Observatory of China in Lijiang (LJ) and the 1.5-m telescope of San Pedro Mártir Observatory of Mexico (SPM). Tables 1 and 2 list the journals of the observations.

In 2007, an observing cycle of 30 seconds was used with the CCD cameras in BOAO and PO, while a three-channel photoelectric photometer (PMT) was used to observe a comparison star, the sky background, and the target simultaneously with the exposure time of 1 second in XL. These PMT data points were then summed to a similar sampling rate of 30 seconds. In 2009 and 2010, CCD cameras were used for all runs with an observing cycle of approximately 30 seconds. 46.1 hours of data were collected in December of 2007 with a duty cycle of 31%, which leads to the frequency

Table 1. Journal of observations in December of 2007. Filter symbols: *B* = Johnson *B*, *W* = white light.

Date	Telescope	Filter	Detector	Hours
7	XL 2.16-m	*W*	PMT	7.03
	PO 1-m	*B*	CCD	0.64
8	XL 2.16-m	*W*	PMT	5.27
	BOAO 1.8-m	*B*	CCD	7.86
9	BOAO 1.8-m	*B*	CCD	7.53
11	XL 2.16-m	*W*	PMT	9.13
	BOAO 1.8-m	*B*	CCD	3.43
12	XL 2.16-m	*W*	PMT	8.00
	PO 1-m	*B*	CCD	0.68
13	XL 2.16-m	*W*	PMT	5.20

Table 2. Journal of observations from December of 2009 to January of 2010. Filter: Johnson *B*.

Date	Telescope	Hours
December 2009		
13	XL 2.16-m	5.18
14	XL 2.16-m	4.86
15	XL 2.16-m	7.15
16	XL 2.16-m	7.09
17	XL 2.16-m	7.10
18	XL 2.16-m	5.49
25	LJ 2.40-m	4.61
26	LJ 2.40-m	5.90
27	LJ 2.40-m	6.00
28	LJ 2.40-m	8.18
29	LJ 2.40-m	2.00
30	LJ 2.40-m	4.36
31	LJ 2.40-m	2.52
January 2010		
12	SPM 1.5-m	5.09
	XL 2.16-m	4.14
13	SPM 1.5-m	5.43
	XL 2.16-m	3.04
14	SPM 1.5-m	5.10
	XL 2.16-m	4.42
15	SPM 1.5-m	5.11
	XL 2.16-m	4.58
16	SPM 1.5-m	3.93
	XL 2.16-m	4.29
17	SPM 1.5-m	5.13
	XL 2.16-m	4.29
24	LJ 2.40-m	5.63
26	LJ 2.40-m	6.10
27	LJ 2.40-m	1.75
28	LJ 2.40-m	2.97
29	LJ 2.40-m	5.38
30	LJ 2.40-m	6.05
31	LJ 2.40-m	5.90

resolution of 1.9 μHz. In 2009-2010 we obtained 158.9 hours of data with a duty cycle of 13.4% and a better frequency resolution of 0.23 μHz.

The CCD data were reduced with the iraf Daophot package. The PMT data were reduced as described in Pfeiffer et al. (1996). Unfortunately the weather conditions were poor at Piszkéstető Observatory during the campaign in 2007, so these data were not included in the final light curves of the year.

The data collected in both BOAO and XL in December 8 and 11 overlapped partially each other. As they were obtained through different filters, Johnson *B* for BOAO and white light for XL, the overlapping data were used to calculate the amplitude ratio obtained between the two time-series. Then, the magnitudes of the light curves from XL were calibrated to those in the filter *B*. Hence, data from the two sites were able to be combined together for frequency analysis. Since the noise level of the PMT data was in general higher than that of the CCD data, the overlapping PMT data were not used for the analysis of the light curves. Fig. 1(a) and (b) show the calibrated light curves of HS 0507+0434B in 2007 and 2009-2010, respectively.

3   THE AMPLITUDE SPECTRUM

We used the `PERIOD04` software (Lenz & Breger 2005) to analyse the light curves and derive the frequencies, amplitudes and phases of the peaks in the Fourier Transforms. The amplitude spectra of the light curves in 2007 and 2009-2010 are shown in the upper panels of Fig. 2(a) and (b), respectively. The amplitude spectra of a sinusoidal function sampled at the same rate as the data and having an amplitude equals to unity when there are data and equals to zero in the gaps (the window functions) are shown in the insets of upper panels of Fig. 2(a) and (b).

From the Fourier Transform (FT) of the light curves in 2007, we extracted frequency values of the highest peaks with `PERIOD04`, fitting the light curves with the frequencies then prewhitenning the corresponding sinusoidal function to look for the next frequencies with significant peaks in the FT. For the peaks extracted, we followed the criterion of Breger et al. (1993) and Kuschnig et al. (1997) to take the peaks whose signal-to-noise (S/N) ratios are higher than 4.0. Finally, 19 significant frequencies were detected from the light curves collected in 2007. The first two columns of Table 3 list the resolved frequencies and their amplitudes in 2007. In the bottom panel of Fig. 2(a) is shown the FT of the residuals after prewhitenning the 19 frequencies.

For the light curves obtained from December of 2009 to January of 2010, we note that the amplitude spectra of the four weeks of light curves differ significantly from each other, especially for the amplitude values of the peaks. Fig. 3 shows the FTs of the light curves of the four individual weeks (namely Week1, Week2, Week3, and Week4, respectively). We discuss those amplitude variations in more details in §5.

To extract the frequency values from the FT of the combined light curves from December of 2009 to January of 2010, we made an analysis similar to the one used to analyse the light curves of 2007. However, since the amplitude of a given peak is varying from week to week, prewhitenning of each of the peak by one frequency with a unique fitted amplitude and phase does not allow to completely remove that sinusoidal function for all the four weeks of light curves. The existence of a residual of the prewhitenning by a sinusoidal function creates a secondary peak whose frequency value is very close to that of the resolved frequency with a lower amplitude. In order to make complete prewhitenning, we optimized the amplitude of each frequency for individual weeks of light curves and then prewhitenned the corresponding sinusoidal functions with varying amplitude values. This process helps us to
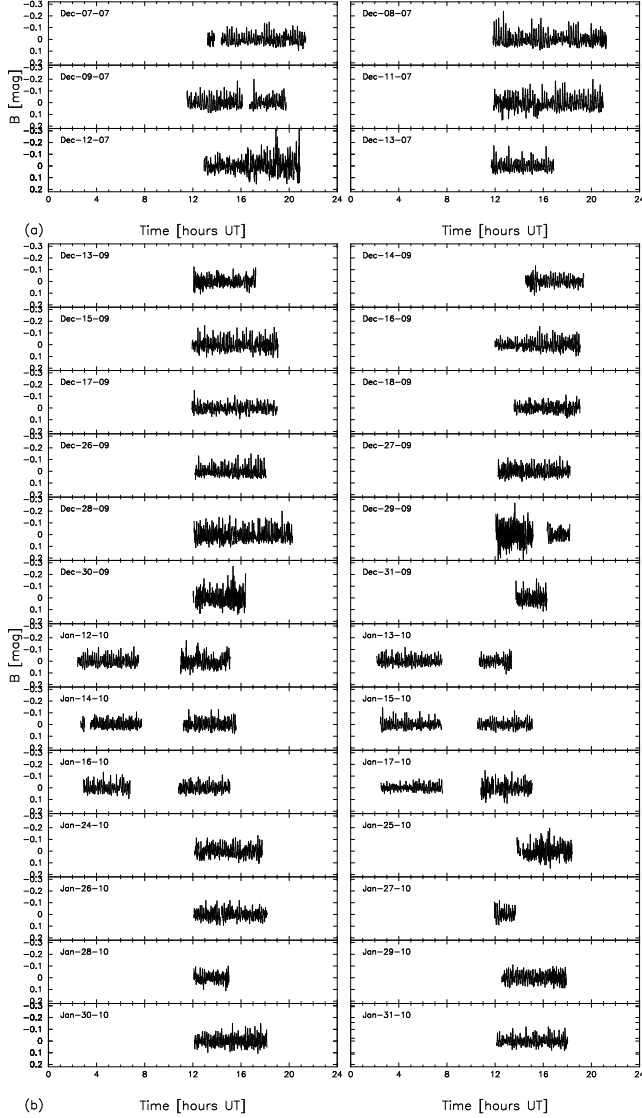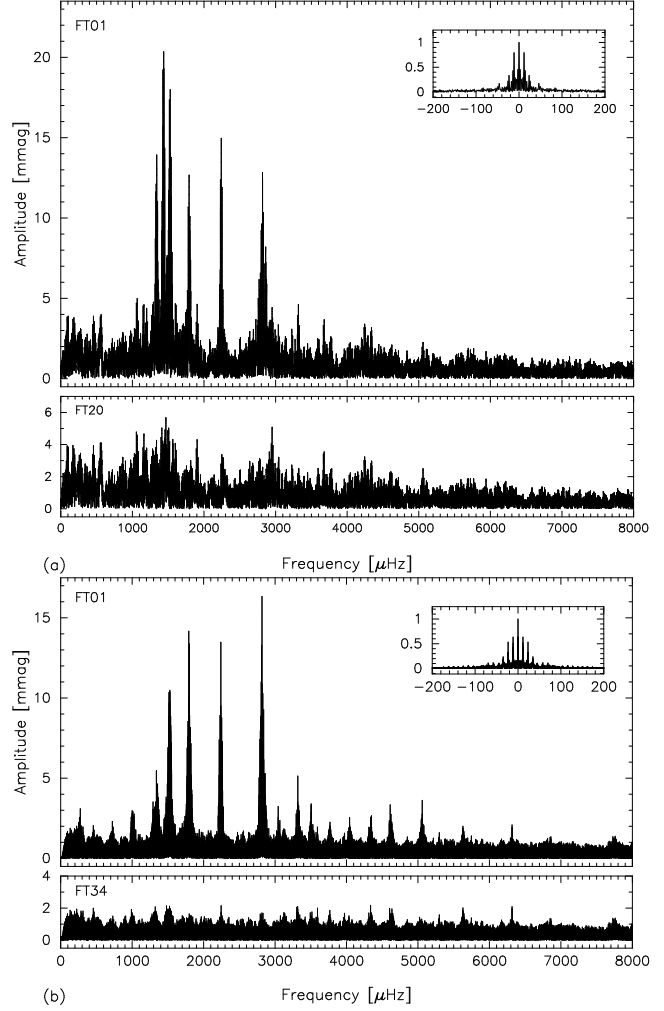
Figure 1. Normalized light curves for HS 0507+0434B in (a) December 7-13, 2007; (b) from December 13, 2009 to January 31, 2010. Each panel covers a 24 h period. The date is indicated on the up-left side inside the panels.

Figure 2. Amplitude spectra of the light curves and the residuals after prewhitenning the detected frequencies in (a) 2007; and (b) 2009-2010 shown in the upper and bottom panels, respectively. The amplitude, in units of milli-magnitude amplitude (mmag), is shown as a function of the frequency in μHz in the frequency range 0-8000 μHz; outside this frequency range no significant signal is detected. The insets are the spectral windows of the data. Please note that the insets and the figures are in different scales.

extract 33 frequencies, that are listed in the third column of Table 3 while the fourth column gives the average amplitude values. The FT of the residuals after prewhitening by the 33 frequencies is shown in the bottom panel of Fig. 2(b). We used the same selection criterion of S/N ratios higher than 4.0 as for the analysis of the 2007 data. As the uncertainties derived by `PERIOD04` estimate the internal consistency of the solutions, they are believed to be underestimated. We derived more realistic uncertainties through Monte-Carlo simulations.

For each observed time-series $(t_i, x_i)_{i=1,2,...,k}$, we extracted a number of frequencies $(f_j)_{j=1,2,...,n}$ and the corresponding amplitudes A_j and phases ϕ_j with the software `PERIOD04`, so the residual time-series $(t_i, y_i)_{i=1,2,...,k}$ were obtained by subtracting the sum of multiple sine functions from the observed time-series as

$$y_i = x_i - \sum_{j=1,2,...n} A_j \sin(2\pi f_j t_i + \phi_j)$$

Then $|y_i|$ is regarded as the observation error of x_i. Hence, we constructed 50 simulated time-series z_i for each observed time-series, by taking z_i as a normally distributed random variable with mean x_i and standard variation $|y_i|$. The 50 simulated time-series were fitted with the sum of multiple sine functions by taking $(f_j, A_j, \phi_j)_{j=1,2,...,n}$ as initial values according to least-squares algorithm. Hence 50 sets of new $(f_j, A_j, \phi_j)_{j=1,2,...,n}$ were obtained. The standard deviations of each parameter of $(f_j, A_j, \phi_j)_{j=1,2,...,n}$ were then calculated. We define them as the uncertainty estimate of the parameters and include those of frequencies and amplitudes in Table 3.

We compared the uncertainties derived from Monte-Carlo simulations with those derived from `PERIOD04` in order to estimate by how much `PERIOD04` underestimates those uncertainties. For the 2007 data set, the average uncertainties on the frequencies and on the amplitudes derived from our Monte-Carlo simulations are
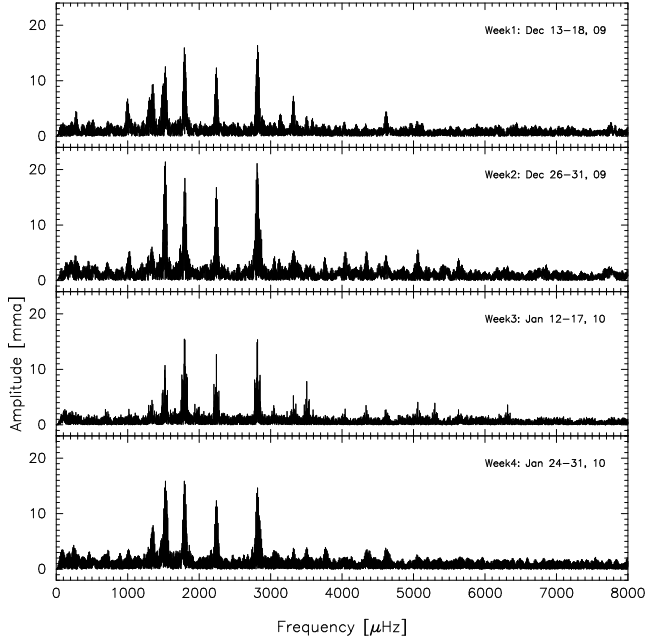
Figure 3. Amplitude spectra of the four weeks of light curves from December 2009 to January 2010. Note the significant differences of the amplitudes of the peaks between the four weeks.

70% larger than those estimated from `PERIOD04`. For the 2009-2010 data sets, `PERIOD04` underestimates the frequency uncertainties by 81% and the amplitude uncertainties by 48%, in average.

4 ASTEROSEISMOLOGY OF HS0507+0434B

4.1 Pulsation frequencies and linear combinations

As shown in Table 1, the useful data for HS 0507+0434B obtained in 2007 were collected within one week from XL and BOAO, which are only one hour apart in longitude. This leads to a strong one-day aliasing effect in the FT, as seen in the window function shown in the inset of Fig. 2(a). For the four-week data-set collected from December 2009 to January 2010 (Table 2), there are three weeks of observations made from single sites. Hence, the one-day aliasing peaks persist in the FT, as seen in the window function shown in the inset of Fig. 2(b), but with a smaller 11.5 μHz component.

Since HS 0507+0434B lies in the middle of the ZZ Ceti instability strip, where the convection-pulsation interaction starts to become important, we anticipated to find many linear combinations of a few independent frequencies as in Handler et al. (2002). We carefully searched for independent frequencies and their linear combinations, taking into account possible remaining aliasing effect and residuals of amplitude variation on the frequency determination.

Table 4 lists the frequencies, amplitudes and periods resulting from our analysis. When the same frequencies occur in the both sets of data (2007 and 2009-2010), we choose the 2009-2010 values since the frequency resolution is better for this data set. In this case, the listed amplitude is the amplitude averaged on the four weeks of the 2009-2010 runs. We searched systematically for linear combination relationship among three frequencies A,B and C such that:

$$f_A \pm \sigma_A = f_B \pm \sigma_B \pm f_C \pm \sigma_C$$

Table 3. Signals detected from the light curves of HS 0507+0434B in 2007 and 2009-2010. f=frequency in μHz. A=amplitude in mmag. The 1σ uncertainties are estimated from Monte-Carlo simulations.

f	A	f	A
(2007)		(2009-2010)	
		274.983 ± 0.018	3.12 ± 0.44
		723.231 ± 0.024	2.34 ± 0.55
		1000.262 ± 0.019	3.04 ± 0.57
		1028.558 ± 0.035	2.83 ± 0.45
		1292.371 ± 0.015	3.90 ± 0.62
1332.797 ± 0.099	10.86 ± 1.14		
1335.831 ± 0.148	10.51 ± 1.17		
1340.241 ± 0.078	12.98 ± 0.82	1340.716 ± 0.011	4.50 ± 0.64
		1351.176 ± 0.046	2.55 ± 0.41
		1355.893 ± 0.008	4.16 ± 0.54
1420.664 ± 0.240	9.06 ± 1.15		
1429.478 ± 0.075	15.19 ± 1.05		
1437.551 ± 0.053	17.43 ± 1.04		
		1476.397 ± 0.012	3.38 ± 0.54
		1519.086 ± 0.019	5.32 ± 0.50
		1521.827 ± 0.004	10.58 ± 0.56
1524.484 ± 0.074	12.67 ± 1.02	1524.559 ± 0.015	5.84 ± 0.59
1528.924 ± 0.042	24.13 ± 1.50	1527.296 ± 0.006	11.04 ± 0.64
		1529.134 ± 0.012	4.66 ± 0.53
1541.309 ± 0.090	13.61 ± 1.39		
		1549.485 ± 0.072	2.76 ± 0.44
1792.277 ± 0.073	14.93 ± 0.87	1792.809 ± 0.003	14.95 ± 0.58
1796.882 ± 0.219	5.03 ± 0.99	1796.841 ± 0.010	6.73 ± 0.51
1801.518 ± 0.105	10.87 ± 0.92	1800.841 ± 0.005	14.26 ± 0.63
		1802.138 ± 0.057	2.07 ± 0.39
2241.497 ± 0.069	14.71 ± 1.10	2241.642 ± 0.004	13.83 ± 0.45
		2248.724 ± 0.014	5.29 ± 0.51
2770.036 ± 0.142	6.85 ± 1.10		
2810.513 ± 0.112	8.46 ± 0.98	2810.768 ± 0.006	12.55 ± 0.46
		2814.219 ± 0.028	2.51 ± 0.52
2817.649 ± 0.076	12.30 ± 0.88	2817.728 ± 0.004	15.81 ± 0.59
2859.908 ± 0.164	6.39 ± 1.00		
2861.801 ± 0.153	8.26 ± 0.91	2861.726 ± 0.017	4.21 ± 0.50
		3043.694 ± 0.018	3.34 ± 0.47
3318.634 ± 0.178	4.64 ± 0.97	3318.685 ± 0.014	5.10 ± 0.59
		3505.943 ± 0.037	3.47 ± 0.54
		3768.946 ± 0.024	2.32 ± 0.39
		4042.533 ± 0.041	2.53 ± 0.41
		4349.907 ± 0.026	2.66 ± 0.50
		4610.526 ± 0.018	3.28 ± 0.51
		5059.364 ± 0.023	3.60 ± 0.51

We select as possible linear combinations only those combinations with:

$$\sigma_A \leqslant 3 \times [\sigma_B + \sigma_C]$$

For every linear combination found, we identify the higher amplitude peaks as independent signals and the lowest one as the combination. We also list as further signals, a number of frequencies of low amplitude which are more uncertain detections at the limit of our selection criterion and/or which are close to possible linear combinations but do not fulfill our $3 \times \sigma$ criterion. Among those frequencies, we discuss two particular cases as follows. The 723.23 μHz which we identify here as a linear combination f_{13}-f_{23} within $3 \times \sigma$ could also correspond to a genuine mode. This will be discussed in section 6. The 1292.37 μHz that is listed as a linear combination does not fulfill our amplitude selection criterion since its presumably parent mode f_{17} has a smaller amplitude. However it fulfills the frequency criterion within $0.6 \times \sigma$. We suggest that the

linear combinations between the largest amplitude components of the implied two triplets(f_{16} and f_{18} interacting with f_7 and f_9) combine to produce this almost exact linear combination.

In Table 4, we do not include 1541.31 μHz which was only seen in the 2007 data since this peak is regarded as the one-day alias of the dominant peak at 1528.92 μHz. Similarly, we exclude the 1351.17 μHz peak as the alias of the 1340.71 μHz. We also exclude the peak at 1802.14 μHz since it may result from the residual of the amplitude variation of the peak at 1800.84 μHz. We include the 2245.63 μHz from Handler et al. (2002) for completeness. For these reasons, Table 4 contains 39 frequencies while Table 3 contains 41.

In comparing with the results of Handler et al. (2002), we find in common the same two complete triplets centered on 1796 μHz (f_{10},f_{11} and f_{12}) and 2814 μHz (f_{16}, f_{17} and f_{18}), the two $m=\pm1$ components of the triplet centered at 2245 μHz (f_{13} and f_{15}; we do not detect the central component of that triplet in our data but we include the Handler's value in Table 4 as f_{14} for completeness) and the triplet centered on 1335 μHz (f_2, f_3 and f_4) where Handler et al. (2002) detected only one component. In addition we find one more triplet centered on 1524 μHz (f_7, f_8 and f_9) and two frequencies (f_5 and f_6) separated by twice the averaged separation between the components of complete triplets. We interpret these two frequencies as the $m=\pm1$ components of an additional triplet whose undetected central component frequency should be at 1433.51 μHz. The lowest frequency f_1 must be a genuine mode since we do not identify any linear combination reproducing this value. By contrast with Handler's results, we do not find as many linear combination frequencies satisfying our S/N selection criterion.

4.2 Period distribution and average period spacing

From Table 4, one finds that the 18 independent signals consist of 6 triplets (with the one central mode missing in the triplet between f_5 and f_6 as mentioned earlier) and 1 single mode. Since we do identify only triplets in the power spectrum, we interpret them as $l = 1$ modes split by rotation. In the asymptotic regime, which we assume here in first approximation, the period separation between modes of same degree l and consecutive orders k should be equal or close to the period spacing. Hence, the observed period separations should correspond to the period spacing, or be approximately its multiples. Examining the periods of the central modes in the triplets and of the single mode, one finds the differences of 251.1 s, 51.0 s, 41.7 s, 99.4 s, 111.2 s, and 90.0 s, respectively. Since the m value of the single mode is not determined, we used the periods of the central modes of the triplets to calculate the average period spacing. This leads to the average period spacing of ΔP=49.63 s.

The period distribution of the $m = 0$ modes allows us to assign an arbitrary δk value to the $m = 0$ modes taking the frequency 2814.22 μHz (period 355.3 s) as the reference δk=0. Table 5 lists the frequencies, the frequency separations, the periods, the δk and the m values for the identified l=1 modes. A straight-line fit to the periods of the six $m = 0$ modes yields the formula,

$$P_k = P_0 + \Delta P \times \Delta k$$

where one gets P_0=353.18±4.12 s and ΔP=49.63±0.78 s. Hence, DP=P-P$_k$ are derived for the six $m = 0$ modes and listed in Table 5.

Fig. 4 shows the linear least-square fit of the six $m = 0$ modes, which confirms the period spacing of ΔP=49.63 s. In addition, by checking the periods listed in Table 4, one finds that the differences

Table 4. Signals identified for HS 0507+0434B. f=frequency in μHz. A=amplitude in mmag. P=Period in second.

ID	f	A	P
	Independent signals		
f_1	1000.26	3.04	999.7
f_2	1332.80	10.86	750.3
f_3	1335.83	10.51	748.6
f_4	1340.24	12.98	746.1
f_5	1429.48	15.19	699.6
f_6	1437.55	17.43	695.6
f_7	1521.83	10.58	657.1
f_8	1524.56	5.84	655.9
f_9	1527.30	11.04	654.8
f_{10}	1792.81	14.95	557.8
f_{11}	1796.84	6.73	556.5
f_{12}	1800.84	14.26	555.3
f_{13}	2241.64	13.83	446.1
f_{14}	[a]2245.63	2.8	445.3
f_{15}	2248.72	5.29	444.7
f_{16}	2810.77	12.55	355.8
f_{17}	2814.22	2.51	355.3
f_{18}	2817.73	15.81	354.9
	Further signals		
f_{19}	1028.56	2.83	972.2
f_{20}	1355.89	4.16	737.5
f_{21}	1420.66	9.06	703.9
f_{22}	1476.40	3.38	677.3
f_{23}	1519.09	5.32	658.3
f_{24}	1529.13	4.66	654.0
f_{25}	1549.48	2.76	645.4
f_{26}	2861.80	8.26	349.4
f_{27}	3505.94	3.47	285.2
f_{28}	4349.91	2.66	229.9
	Linear combinations		
$f_{11} - f_7$	274.98	3.12	3636.6
$f_{13} - f_{23}$	723.23	2.34	1382.7
$f_{17} - f_7$	1292.37	3.90	773.8
$f_2 + f_6$	2770.04	6.85	361.0
$f_3 + f_8$	2859.91	6.39	349.7
$f_7 + f_7$	3043.69	4.34	328.5
$f_7 + f_{11}$	3318.68	5.10	301.3
$f_9 + f_{13}$	3768.95	2.32	265.3
$f_{12} + f_{13}$	4042.53	2.53	247.4
$f_{10} + f_{18}$	4610.53	3.28	216.9
$f_{13} + f_{18}$	5059.36	3.60	197.7

[a] From Handler et al. (2002).

between the period of f_{17} (whose m value is 0) and the periods corresponding to the three frequencies of 3318.68, 4042.53, and 5059.36 μHz (301.3 s, 247.4 s and 197.7 s respectively), which we interpret as linear combinations, are 54.0, 53.9, and 49.7 s, respectively. Hence, the periods of these three linear combinations fit surprisingly well the period spacing of 49.63 s. One may wonder whether these linear combination frequencies coincide with genuine $l = 1$ modes of lower order. We will discuss this point further in §6.

Table 5. Period distribution in HS 0507+0434B. f=frequency in μHz. P=Period in second. δf=frequency separation among a triplet in μHz. DP are the residuals of the fit to the periods of the six $m = 0$ modes. The frequency indicated in *italic* is estimated from the average frequency of the two components $m=\pm 1$ of the triplet.

f	δf	P	δk	m	DP
1332.80		750.3		-1	
	3.03				
1335.83		748.6	+8	0	-1.65
	4.41				
1340.24		746.1		+1	
1429.48		699.6		-1	
	4.03				
1433.51		*697.6*	+7	*0*	-3.02
	4.03				
1437.55		695.6		+1	
1521.83		657.1		-1	
	2.73				
1524.56		655.9	+6	0	4.92
	2.74				
1527.30		654.8		+1	
1792.81		557.8		-1	
	4.03				
1796.84		556.5	+4	0	4.78
	4.00				
1800.84		555.3		+1	
2241.64		446.1		-1	
	3.99				
2245.63		445.3	+2	0	-7.15
	3.09				
2248.72		444.7		+1	
2810.77		355.8		-1	
	3.45				
2814.22		355.3	0	0	2.12
	3.51				
2817.73		354.9		+1	

### 4.3 Rotational splitting and rotation rate

We interpret the 6 triplets identified in the FT as $l = 1$ modes split by rotation. Column 2 of Table 5 lists the frequency separation between the rotationally split components, $m=\pm 1$, and the central component, $m=0$, for the 6 triplets. We derive an average value of frequency separation between the outer two components of the triplets as **3.59$\pm$0.57 μHz.** To the first order in the rotation angular frequency Ω, the frequencies in the rotating case $\sigma_{k,l,m}$ are related to the frequencies in the non-rotating case $\sigma_{k,l}$ by:

$$\sigma_{k,l,m} = \sigma_{k,l} + m \times (1 - C_{k,l})\Omega$$

with $C_{k,l} = 1/l(l + 1)$ in the asymptotic regime (Brickhill 1975). Assuming that it is the case of the pulsations observed in HS 0507+0434B, we derive an average rotation period of **1.61**$\pm$0.26 **days.** This value is in agreement with the rotation period derived by Handler et al. (2002) of 1.70$\pm$0.11 days within the uncertainties.

4.4 The angle of the rotation axis to the line of sight

Among the five triplets (the sixth one with central mode missing is not included) listed in Table 4, one may find that four of them show weaker central modes ($m = 0$) obviously than the $m = -1$ and
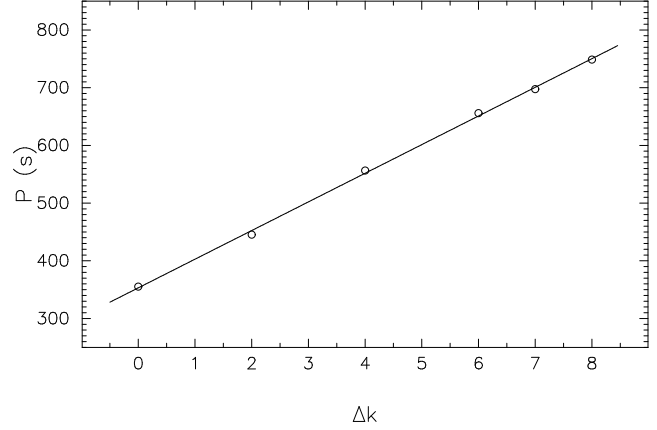

Figure 4. Linear least-square fit of the six $m = 0$ modes (open circles) as a function of Δk, the differences in radial order from the reference mode. The fit confirms a period spacing ΔP=49.63 s.

$m = +1$ modes in the same triplets. Making the assumptions that the pulsation axis is aligned with the star rotation axis and that the average amplitudes ratios of the components within the multiplets are due to geometrical effects only, it is possible to infer the angle of the rotation axis on the line of sight. We hence calculate the ratio of the average amplitudes of the $m = \pm 1$ to that of the amplitudes of the $m = 0$ modes for the four triplets. The result is 1.98. This implies that the angle of the rotation axis to the line of sight is close to 70 ° (Pesnell 1985). However, we note that the fifth triplet centered on 1335.8 μHz has its three components of similar amplitude. Either these particular pulsation modes have a different symmetry axis than the other four triplets, or the amplitude ratios are not only due to geometrical effect. The full triplet was seen in 2007 while only the prograde component was detected in 2009-2010 with an amplitude reduced by a factor 3. Those amplitude variations, seen for other modes as well, are discussed below in §5. They suggest that the amplitude ratio cannot be simply explained by geometrical effect.

4.5 Mode trapping

With the linear least-square fit of the periods of the six $m = 0$ modes, we calculate the residuals of these six periods relative to the linear fit with the average period spacing of 49.63 s. Fig. 5 plots the residuals versus the periods, which shows evidence of mode trapping. The two modes with periods of 445.3 s and 697.6 s show the largest deviations from the average period spacing. Both shoud be trapped modes or close to trapped modes. They are separated in periods by five times the average period spacing, i.e. five modes. This is a preliminary indication of a trapping by a thin hydrogen layer. Brassard et al. (1992) and Kawaler & Bradley (1994) have shown that the distance in periods, and consequently the number of modes, between trapped modes increases as the surface hydrogen layer becomes thinner. In the mean time, from the linear theory of pulsation, the trapped modes are expected to have the largest amplitudes since they have the largest growth-rates. However, this has been shown not to be true in many cases: for instance in PG 1159-035 (Winget et al. 1991), in GD 358 (Winget et al. 1994), in RXJ 2117+3412 (Vauclair et al. 2002), in EC 14012-1446 (Provencal et al. 2012). In HS 0507+0434B as in those other pulsators, there is no correlation between the amplitudes of the modes and their trapped or untrapped status, indicating that the amplitudes
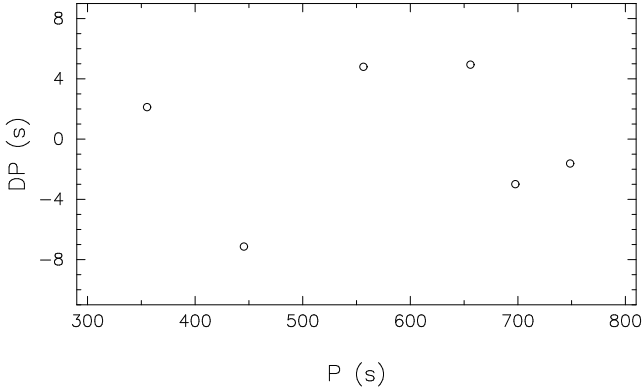
Figure 5. A plot showing observational evidence of mode trapping. The residuals of the period distribution relative to the average period spacing (ΔP=49.63 s) are plotted as a function of the period. The open circles represent the $m = 0$ modes of the six triplets. The modes with periods of 445.5 s and 697.6 s defining clear minima on this plot should be trapped modes.

are not simply governed by their linear growth-rate. Amplitude and frequency variations, as discussed below in section 5, may be the reason why the triplet at 1433 μHz is not detected in the 2009-2010 data set in spite of being a probable trapped mode.

5 THE AMPLITUDE VARIATION

By comparing the upper panel of Fig. 2(a), the four panels of Fig. 3, and Fig. 3 of Handler et al. (2002) based on one-week single-site CCD photometric observations in 2000, one finds quite different amplitude spectra. As mentioned in §3, we had to optimize the amplitude values of the same frequencies for the four different weeks of light curves from December 2009 to January 2010 when we extracted frequencies from the FT of the combined light curves. Fig. 6 shows the amplitude variations of the 33 frequencies. Table 6 lists the 33 frequencies and their amplitudes during the four individual weeks. We checked that for each of the four weeks, the achieved frequency resolution allows to resolve the rotational splitting. The frequency resolution is 2.2 μHz, 1.9 μHz, 2.1 μHz and 1.6 μHz for week1,week2, week3 and week4 respectively while the rotational splitting is 3.6 μHz. This indicates that the observed amplitude variations are real and are not due to the beating between the components within the triplets.

The "pulsation power" of HS 0507+0434B during the four individual weeks is estimated in $mmag^2$ per second by computing:

$$E = \sum_{i=1}^{33} f_i \times A_i^2$$

The results are listed in the bottom of Table 6. A similar estimate for the 2007 data set gives E= 5.11 $mmag^2$ per second. These results suggest that the "pulsation power" is time-dependent. HS 0507+0434B was pulsating more vigorously during our 2007 run and during the week2 of December 2009 than during the other three weeks of December 2009 and January 2010 where the "pulsation power" was almost constant.

Amplitude variations are not uncommon among pulsating white dwarfs. They have been noticed, for instance, in the ZZ Ceti pulsators KUV 02464+3239 (Bognár et al. 2009), EC 14012-1446 (Provencal et al. 2012), WDJ 1916+3938 (Hermes et al. 2011), in the DBV prototype GD 358 (Kepler et al. 2003, Provencal et al.

Table 6. Frequencies extracted from the combined light curves from December 2009 to January 2010 and the amplitudes optimized for the four individual weeks. f=frequency in μHz. A=amplitude in mmag. E represents the pulsation power in $mmag^2$ per second of the star in the four individual weeks (see the text for the details).

| ID	f	Week1	Week2	Week3	Week4
			A		
F_{01}	274.98	3.27	3.57	2.23	3.38
F_{02}	723.23	2.66	1.06	2.44	3.46
F_{03}	1000.26	5.42	4.05	1.03	3.11
F_{04}	1028.56	3.05	4.70	1.88	1.16
F_{05}	1292.37	5.42	4.02	3.53	3.43
F_{06}	1340.72	5.80	3.43	3.23	5.04
F_{07}	1351.18	3.60	2.47	2.34	5.83
F_{08}	1355.89	9.20	3.62	0.49	7.28
F_{09}	1476.40	7.12	2.09	1.94	4.26
F_{10}	1519.09	2.20	5.93	5.12	6.91
F_{11}	1521.83	8.50	9.64	10.32	14.19
F_{12}	1524.56	2.29	5.39	4.64	7.43
F_{13}	1527.30	9.82	20.12	1.23	11.97
F_{14}	1529.13	6.94	1.87	6.05	6.17
F_{15}	1549.48	2.41	3.23	3.36	7.86
F_{16}	1792.81	16.93	13.97	14.22	16.81
F_{17}	1796.84	6.70	8.18	5.27	5.08
F_{18}	1800.84	12.05	19.95	15.54	10.34
F_{19}	1802.14	3.91	2.21	2.95	4.54
F_{20}	2241.64	12.84	16.41	13.12	12.43
F_{21}	2248.72	4.80	8.63	5.49	3.07
F_{22}	2810.77	9.07	20.16	15.04	6.35
F_{23}	2814.22	2.08	3.10	2.37	3.36
F_{24}	2817.73	15.49	18.23	15.77	14.28
F_{25}	2861.73	4.07	5.82	2.37	4.69
F_{26}	3043.69	2.81	4.03	3.30	3.26
F_{27}	3318.68	6.75	5.50	5.36	3.58
F_{28}	3505.94	3.11	1.97	7.54	2.44
F_{29}	3768.95	1.57	3.24	1.66	2.81
F_{30}	4042.53	1.32	4.80	2.86	0.91
F_{31}	4349.91	0.60	4.96	1.72	3.06
F_{32}	4610.53	4.36	4.04	2.29	3.48
F_{33}	5059.36	2.55	5.35	4.09	2.30
			E		
		3.31	5.78	3.54	3.23

2009) as well as in the GW Virginis star PG 0122+200 (Vauclair et al. 2011). Such amplitude variations associated with frequency variations are expected in the case of resonant coupling induced by the rotation within multiplets (Goupil et al. 1998). The interaction of the pulsation with convection could also be invoked as the cause for the amplitude and "pulsation power" variability. More observational data and theoretical investigations are needed to explore the physical causes of those variabilities. This is out of the scope of the present paper.

6 CONSTRAINTS FROM THE THEORETICAL MODELS

We computed a grid of DA white dwarf models in a range of the 4 parameters : $0.54 < M/M_\odot < 0.75$, $2.5\times10^{-3} < L/L_\odot < 6.3\times10^{-3}$, $-10 < log q_H < -4$, where $q_H = M_H/M_*$ is the hydrogen mass fraction and for the helium mass fraction $10^{-4} < M_{He}/M_* < 10^{-2}$. In this preliminary modeling, we use the ML2 version of the mixing-length "theory" to describe the convection with the value of the
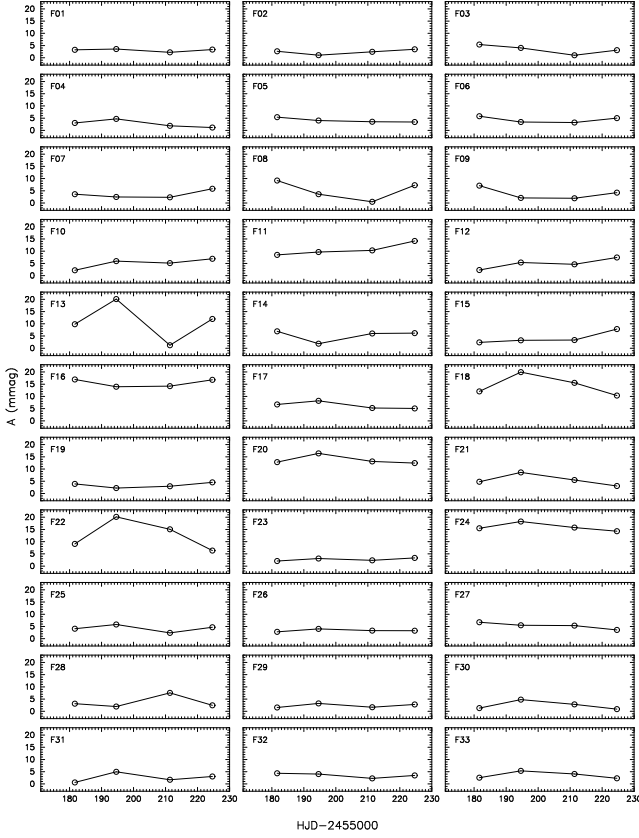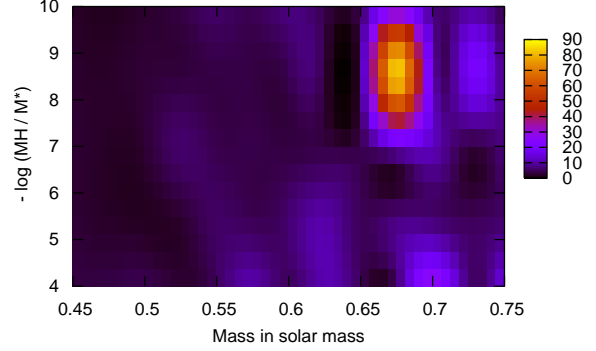
Figure 6. Amplitude variations of the 33 frequencies among four weeks of December of 2009 and January of 2010 in HS 0507+0434B.

Figure 7. Least square fit of oscillations of HS0507+0434B compared with models: 2D cut in the $-\log(M_H/M_*)$ versus $M_*/M_\odot$ of the complete 4D parameters domain. The contour maps show the iso-inverse χ^2 of the fits. The lowest value of the contours is for $1/\chi^2$ equals to 5. The next contours are shown from 10 to 80 by step of 10. The best fit model corresponds to the value of $1/\chi^2$ equals to 88.

Table 7. Fit of the computed periods with the periods observed in HS 0507+0434B in 5 different stellar models; the first column is the model number; the following three columns give the total mass, the luminosity and the hydrogen mass fraction of each model; the last column gives the inverse χ^2 of the fit. Model 4 is selected as the best fit model.

Model	$M_*/M_\odot$	$L_*/L_\odot(10^{-3})$	$log(M_H/M_*)$	$1/\chi^2$
1	0.700	3.2	-4.0	25
2	0.675	3.3	-4.0	23
3	0.675	3.4	-8.5	44
4	0.675	3.5	-8.5	88
5	0.675	3.6	-8.5	42

mixing-length parameter $\alpha= 0.6$, following Bergeron et al. (1995). The models are assumed to have reached the equilibrium chemical stratification through the effect of gravitational settling. Their degenerate core is a homogeneous mixture of carbon and oxygen. For each model of the grid, we computed the periods of the adiabatic g-mode oscillations for the degree $\ell=1$ and for orders $k = 1$ to 27. A χ^2 is computed from the comparison of these periods with the observed periods of the $m = 0$ central components of the 6 triplets listed in Table 5.

Figure 7 shows a 2D slice in a $-\log(M_H/M_*)$ vs $M_*/M_\odot$ plane with the values $M_{He}/M_* = 10^{-2}$, $L/L_\odot=3.5\times10^{-3}$, which correspond to the values of these two parameters for which we obtain the best fit in the complete 4D parameter grid. The best fit model is identified as the one with the lower χ^2. For a better visibility $1/\chi^2$ is shown on the figure; the best-fit model has a $1/\chi^2=$ 88. The best model obtained in the grid corresponds to $M_*/M_\odot =$ 0.675, $L/L_\odot=3.5\times10^{-3}$, $M_H/M_*= 10^{-8.5}$. Its effective temperature, 12460 K, is in good agreement with the new spectroscopic estimate of Gianninas et al. (2011) of 12290 ±186 K. The inferred thin hydrogen layer is in agreement with the mode trapping discussed above in section 4.5. This low value of the hydrogen mass fraction suggests that HS 0507+0434B has evolved from a last He thermal pulse during which the H is efficiently burned (Althaus et al. 2005).

Our results are in good agreement with the analysis of Romero et al. (2012) for the total mass and the luminosity ($M_*/M_\odot= 0.660$ and $L/L_\odot= 2.95\times 10^{-3}$) but disagrees on the hydrogen mass fraction for which Romero et al. (2012) find $M_H/M_*= 5.7\times10^{-5}$. Note that in their analysis, Romero et al. used the periods of the 4 triplets listed in Castanheira & Kepler (2009), taken from the study of Han-

dler et al. (2002). In the present paper we use two more triplets. Note also that our present result for the hydrogen mass fraction is in disagreement with our previous preliminary analysis (Fu et al. 2010) in which we also found a best fit for a "thick" hydrogen layer ($M_H/M_* = 10^{-4.4}$). However, in this previous study we introduced the 301 s period in the fit while we are now confident that this period results from a linear combination and is not a genuine mode. In addition, the χ^2 analysis in the 4D parameter space exhibits many minima; our present fits also show a minimum at the previous value of $M_H/M_* = 10^{-4.4}$ but with a much higher χ^2 value than the one we now find for $M_H/M_*= 10^{-8.5}$. The value derived in Fu et al. (2010) comes most probably from the identification of a secondary minimum of the χ^2.

In estimating the inverse χ^2 values for the series of model of our grid, we do find maxima which sometimes correspond to "thick" hydrogen layer models. Table 7 summarizes the parameters of the five models which give the best fits among the models computed in our grid. f Figure 8 shows the residuals to the average period spacing of the periods computed in each of the five models, from model 1 in the top panel to model 5 in the bottom panel. All the $\ell=1$ g-mode periods of the models are shown in the range of periods corresponding to the observed ones, i.e. between 300 s and 750 s. They correspond to radial order k from 4 to 14 for the "thick" hydrogen layer models 1 and 2 and k from 2 to 10 for the

Table 8. Preliminary identification of the modes observed in HS 0507+0434B. P_{obs} are the observed periods in seconds, P_{model} the closest periods of the best fit model with their degree ℓ, order k and azimutal number m.

P_{obs}	P_{model}	ℓ	k	m
197.7	198.8	2	2	?
354.9				+1
355.3	357.9	1	3	0
355.8				-1
444.7				+1
445.3	449.2	1	5	0
446.1				-1
555.3				+1
556.5	560.5	1	7	0
557.8				-1
654.8				+1
655.9	654.6	1	8	0
657.1				-1
695.6				+1
697.6	689.9	1	9	0
699.6				-1
703.9	703.3	2	18	?
746.1				+1
748.6	746.0	1	10	0
750.3				-1
972.2	972.8	2	26	?
999.7	986.9	2	27	?
1382.7	1383.0	2	38	?

"thin" hydrogen layer models 3, 4 and 5. The dotted lines indicate the periods of the central component of the six observed triplets.

The observations indicate that the 445 s and the 698 s periods correspond to trapped or "almost trapped" modes. In the "thick" hydrogen layer model 1, these periods would best correspond to the modes of order k= 7 and 13, respectively, which are not trapped modes. In model 2, the period fit is the worst and the mode (k=7) with the closest period to the observed 445 s does not correspond to a trapped mode.

In each of the "thin" hydrogen layer models 3, 4 and 5, the computed most trapped mode is found for the order k=6, with a period of 500.7 s, 491.7 s and 489.8 s, respectively. This mode is not detected in our present data sets. As mentioned in §4.5, the amplitude of a mode is not simply related to its linear growth-rate. So the amplitude of the trapped mode could have been lower than the detection limit during our observing runs. The observed period at 445 s corresponds to the order k=5 next to the trapped mode. The period 698 s corresponds to the order k=9. But in model 3 this is not a trapped mode. The observed trapped or "almost-trapped" modes are in better agreement with the modes computed in model 4 and 5 and the global fit estimated from our inverse χ^2 selects the model 4 as the best-fit model.

This discussion illustrates how sensitive the result is on the number of observed and identified modes. In the data sets presented here, the triplet at 698 s seen in the 2007 data is not present in the 2009-2010 data. In addition, the trapped mode around 500 s that is predicted in our best fit model is absent in both data sets. This justifies the need for a follow up of this ZZ Ceti star in order to find more modes to better constrain the model and conclude unambiguously about the "thick" versus "thin" hydrogen content of that star. However, there are also other arguments in favor of HS 0507+0434B having a "thin" hydrogen layer. HS 0507+0434A+B form a common proper motion system. Both their similar distance, 49 pc and 48 pc respectively (Gianninas et al. 2011) and their similar radial velocity, within their uncertainties (Maxted et al. 2000, their Table 9), confirm that the two stars have been formed together at the same time. However, in spite of their similar mass ($M_*/M_\odot$=0.67 for the A component according to Gianninas et al. and $M_*/M_\odot$=0.675 for the B component from our asteroseismic determination), they show significantly different effective temperature: the component A having 21550 K while the component B, within the same time scale, has cooled to 12290 K (Gianninas et al. 2011). This suggests that HS 0507+0434B should have a thinner hydrogen layer than its companion HS 0507+0434A.

Coming back to the periods at 301.3 s, 247.4 s and 197.7s which we find to fit well the period distribution with the average period spacing of 49.63 s, as discussed in §4.2, we checked that neither of the 247.4 s and 197.7s periods could correspond to genuine ℓ=1 modes since, at least in our claimed "best-fit model", the fundamental ℓ =1; k = 1 mode has a period of 271.7 s. However, we will discuss below the case of the 197.7s as a possible ℓ=2 mode. As far as the 301.3 s is concerned, the corresponding frequency (3318 μHz) is distant by 150 μHz from the closest mode in the best-fit model. As this point, we conclude that our check with the best-fit model confirms these three peaks in the FT as linear combinations.

Finally, having selected one model as the best fit model, we checked a posteriori whether some of the further signals or linear combinations listed in Table 4 could be identified with either ℓ=1 and/or ℓ=2 modes. To do this we computed the periods of the ℓ=2 modes of the best fit model for radial orders k from 2 to 49. We find that some of the further signals could correspond to ℓ=2 modes: this is the case for the 703.9 s period (f_{21}), the 972.2 s period (f_{19}) and the 999.7 s period (f_1) . The 1382.7 s period identified as a linear combination (f_{13} - f_{23}) in Table 4 could as well be identified as a ℓ=2 mode. The 197.7 s identified as another linear combination (f_{13} - f_{18}) could also be identified as the ℓ=2, k=2 mode for which we find a period of 198.8 s. Table 8 summarizes the identifications that can be proposed for as many modes as possible. The observed modes correspond to rather low order k, between 3 and 10 for the ℓ=1 modes. It means that the HS 0507+0434B pulsation spectrum is not entirely in the asymptotic regime. The period distribution does not follow exactly the regular period spacing expected in the asymptotic regime. This explains that while the "trapped modes" are separated by Δk= 5 in Table 5 it is Δk=4 in Table 8.

7 SUMMARY AND CONCLUSIONS

We summarize our results as follows:

- we have obtained new photometric time-series of the ZZ Ceti star HS 0507+0434B in 2007, 2009 and 2010. The combined power spectra allow us to identify 18 independent pulsation modes consisting of 6 triplets and one single mode, plus a number of their linear combinations. We identify those triplets as ℓ=1 g-modes split by rotation.

- we determine an average period spacing of 49.63 s. The period distribution exhibits the signature of mode trapping.
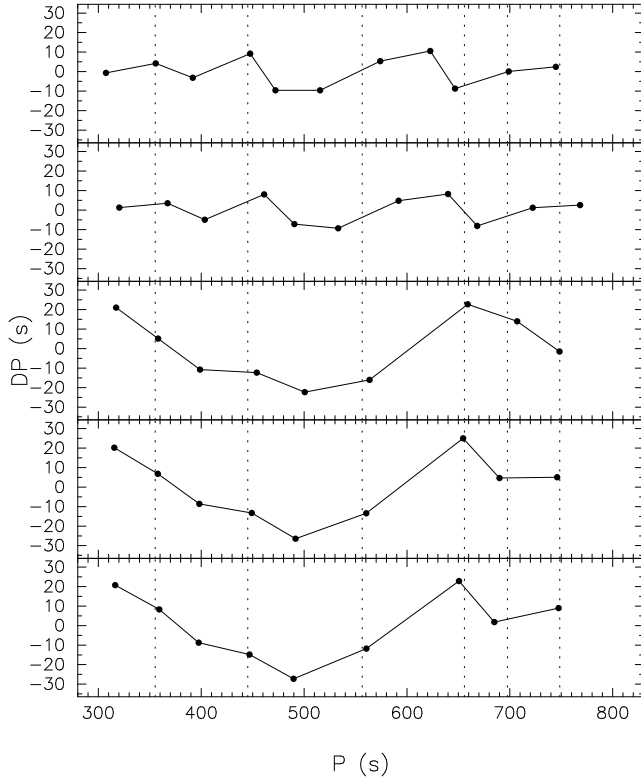
Figure 8. Residuals of the period distribution to the average period spacing for the five best fit models listed in Table 7, from model 1 in the top panel to model 5 in the bottom panel. Dotted lines are the observed periods of the m=0 modes of the six identified triplets. Model 4 gives the best fit in terms of χ^2.

- from the frequency shifts measured in the triplets, we determine an average rotational splitting of 3.59 ±0.57 μHz from which we infer an average rotation rate of 1.61 ±0.26 days. The amplitude ratio of the triplets components, if interpreted as uniquely due to geometrical effect, could be used to estimate that the angle of the rotation axis on the line of sight is close to 70 °. However, the evidence of amplitude variations casts some doubts on the assumption that only geometrical aspect is responsible for the amplitude ratios.

- the amplitude of the modes vary on week time-scale and we find that the "pulsation power" is also time dependent.

- we computed a grid of models and their ℓ=1 g-modes in the adiabatic approximation. The comparison of their theoretical periods with the observed periods through χ^2 tests allows us to estimate the fundamental parameters of a preliminary "best fit" model which has a total mass of $M_*/M_\odot = 0.675$, a luminosity $L/L_\odot$=3.5×10^{-3}, a thin hydrogen outer layer of M_H/M_* = $10^{-8.5}$. The periods of other models with "thick" hydrogen envelope do not fit as well the observed periods according to their χ^2. The "thin" hydrogen envelope of the best fit model of HS 0507+0434B is in agreement with the fact that its common proper motion companion HS 0507+0434A, which must have been formed at the same time and has a similar mass, has a significantly higher effective temperature. This implies that the B component must have a thinner H envelope than the A component for having cooled down to a lower effective temperature during the same cooling time scale. This low value of the hydrogen mass fraction suggests that HS 0507+0434B has evolved from a last He thermal pulse episode.

Further observations of HS 0507+0434B are required to re-fine the modeling, to better constrain the amplitude variation time-scales and identify the physical mechanism driving those variations, and to contribute to the mapping of the convection efficiency through the ZZ Ceti instability strip.

REFERENCES

Althaus, L.G., Serenelli, A.M., Panei, J.A. et al. 2005, A&A, 435, 631

Bergeron, P., Wesemael, F., Lamontagne, R. et al. 1995, ApJ, 449, 258

Bergeron, P. Fontaine, G., Billères, M. et al. 2004, ApJ, 600, 404

Bognár, Zs, Paparó, M., Bradley, P.A., Bischoff-Kim, A. 2009, MNRAS, 399, 1954

Brassard, P., Fontaine, G., Wesemael, F., Hansen, C.J. 1992, ApJS, 80, 369

Breger, M., Stich, J. Garrido, R. et al. 1993, A&A, 271, 482

Brickhill, A.J. 1975, MNRAS, 170, 404

Castanheira, B.G. & Kepler, S.O. 2009, MNRAS, 396, 1709

Castanheira, B.G., Kepler, S.O., Kleinman, S.J. et al. 2010a, 17th European White Dwarfs Workshop, AIP Conference Proceedings, 1273, 500

Castanheira, B.G., Kepler, S.O., Kleinman, S.J. et al. 2010b, MNRAS, 405, 2561

Córsico, A.H., Miller Bertolami, M.M., Althaus, L.G. et al. 2007, A&A, 475,619

Dolez, N. & Vauclair, G. 1981, A&A, 102, 375

Dolez, N., Vauclair, G., Kleinman, S.J. et al. 2006, A&A, 446, 237

Fontaine, G., Bergeron, P., Billères, M. et al. 2003, ApJ, 591, 1184

Fu, J.-N., Vauclair, G., Solheim, J.-E. et al. 2007, A&A, 467, 237

Fu, J.-N., Dolez, N., Vauclair, G. et al. 2010,17th European White Dwarf Workshop,AIP Conference Proceedings, 1273, 516

Gianninas, A., Bergeron, P. & Ruiz, M.T. 2011, ApJ, 743, 138

Goupil, M.-J., Dziembowski, W. & Fontaine, G. 1998, Baltic Astron., 7, 21

Handler, G., Romero-Colmenero, E., Montgomery, M.H. 2002, MNRAS, 335, 399

Harris, H.C., Munn, J.A., Kilic, M. et al. 2006, A.J., 131, 571

Hermes, J.J., Mullally, F., Ostensen, R.H. et al. 2011, ApJ, 741, L16

Jordan, S., Koester, D., Vauclair, G. et al. 1998, A&A, 330, 277

Kawaler, S.D. & Bradley, P.A. 1994, ApJ, 427, 415

Kepler, S.O., Nather, R.E., Winget, D.E. et al. 2003, A&A, 401, 639

Kotak, R., van Kerkwijk, M.H., Clemens, J.C. 2002, A&A, 388, 219

Kuschnig, R., Weiss, W.W., Gruber, R. et al. 1997, A&A, 328, 544

Lenz, P., & Breger, M. 2005, Comm. in Asteroseismology, 146, 53

Maxted, P.F.L., Marsh, T.R. & Moran, C.K.J. 2000, MNRAS, 319, 3051

Montgomery, M.H. 2005, ApJ, 633, 1142

Montgomery, M.H., Provencal, J.L., Kanaan, A. et al. 2010, ApJ, 716, 84

Pesnell, W.D. 1985, ApJ, 292, 238

Pfeiffer, B., Vauclair, G., Dolez, N. et al. 1996, A&A, 314, 182

Provencal, J.L., Montgomery, M.H., Kanaan, A. et al. 2009, ApJ, 693, 564

Provencal, J.L., Montgomery, M.H., Kanaan, A. et al. 2012, ApJ, 751, 91

Redaelli, M., Kepler, S.O., Costa, J.E.S. et al. 2011, MNRAS, 415, 1220

Romero, A.D., Córsico, A.H., Althaus, L.G. et al. 2012, MNRAS, 420, 1462

Ruiz, M.T. & Bergeron, P. 2001, ApJ, 558, 761

Vauclair, G., Moskalik, P., Pfeiffer, B. et al. 2002, A&A, 381, 122

Vauclair, G., Fu, J.-N., Solheim, J.-E. et al. 2011, A&A, 528,5

Winget, D.E., van Horn, H.M., Tassoul, M. et al. 1982, ApJ, 252, 65

Winget, D.E., Hansen, C.J., Liebert, J. et al. 1987, ApJ, 315, L77

Winget, D.E., Nather, R.E., Clemens, J.C. et al. 1991, ApJ, 378, 326

Winget, D.E., Nather, R.E., Clemens, J.C. et al. 1994, ApJ, 430, 839

Wood, M.A. 1995, in White Dwarfs , ed. D. Koester & K. Werner (LNP 443; Berlin; Springer), 41

Wu, Y. 2001, MNRAS, 323, 248